Available online at www.sciencedirect.com
SCIENCE DIRECT®
International Journal of Heat and Mass Transfer 48 (2005) 1283–1292
International Journal of HEAT and MASS TRANSFER
www.elsevier.com/locate/ijhmt

Analysis of a counter-current vapor flow absorber

Nitin Goel, D. Yogi Goswami *

Solar Energy and Energy Conversion Laboratory, Department of Mechanical and Aerospace Engineering, University of Florida, P.O. Box 116300, Gainesville, FL 32611–6300, USA

Received 11 June 2004; received in revised form 2 October 2004
Available online 10 December 2004

Abstract

Analytical investigation of a combined heat and mass transfer process in a counter-current ammonia–water based absorber is presented. The model accounts for both liquid and vapor phase mass transfer resistances, and uses empirical correlations to predict the heat and mass transfer coefficients. The model was used to analyze a lamella plate based absorber with falling film absorption. A finite difference technique was employed to solve the numerical model. It was found that the major portion of the mass transfer resistance lies primarily in the liquid phase. A parametric analysis was also conducted to assess the effect of various parameters on the performance of the absorber.

Keywords: Absorber; Absorption; Falling film; Mass transfer

1. Introduction

Heat driven absorption thermodynamic cycles offer a possibility of generating both power and cooling with environment friendly refrigerants, such as ammonia. The absorber in such systems is one of the critical components in terms of size, efficiency and cost. Absorbers for cycles with nonvolatile absorbents, such as LiBr–water cycle have been studied more extensively as compared to volatile absorbents. In the case of ammonia–water pair, the refrigerant and absorbent are present in both liquid and vapor phases making the transport phenomena more complex to analyze.

Numerical analysis is essential for a thorough understanding and development of an efficient design. Falling film absorbers have been extensively studied over the last few decades. Several investigators have developed computational models to predict the performance of these absorbers. There is a disagreement among researchers regarding the existence of dominant resistance to mass transfer in either liquid or vapor phase [1]. The mass transfer resistance is quite often neglected in either phase to simplify the numerical models [2–10]. Mass transfer resistances in both liquid and vapor phases were considered by Gommed et al. [11,12], Kim [13], Perez-Blanco [14], Potnis et al. [15] and Kang et al. [16,17]. The analysis by Gommed et al. [11,12] and Potnis et al. [15] predicted that the vapor phase mass transfer resistance is dominant, whereas, Kim [13] and Perez-Blanco [14] concluded that the liquid-phase mass transfer resistance controls the overall absorption process. Models developed by Gommed et al. [11,12] and Kim [13] were self-reliant and did not require empirical correlations for heat and mass transfer coefficients. Gommed et al. [11,12] studied falling film absorption on vertical tubes for a co-current vapor flow system.

* Corresponding author. Tel.: +1 352 392 0812; fax: +1 352 392 1071.
E-mail address: goswami@ufl.edu (D.Y. Goswami).

0017-9310/$ - see front matter © 2004 Elsevier Ltd. All rights reserved.
doi:10.1016/j.ijheatmasstransfer.2004.10.009

Nomenclature

A	area, m^2
B	width of the cooling plate, m
C_p	specific heat, kJ/kg K
D_{aw}	volumetric diffusivity, m^2/s
D_h	hydraulic diameter, m
dm	mass flux transferred, kg/s
g	acceleration due to gravity, m/s^2
H	enthalpy, kJ/kg
h	heat transfer coefficient, $kW/m^2 K$
K	mass transfer coefficient, $kmole/m^2 s$
k	thermal conductivity, W/m K
L	length of the cooling plate, m
M	molecular weight, kg/kmol
m	mass flow rate, kg/s
P	total absolute pressure, Pa
Pr	Prandtl number, $\mu C_p/k$
Q	heat transfer, kW
Re_{film}	Reynolds number for falling film, $4\Gamma/\mu$
Re_{film1}	Reynolds number for falling film, $400V/Bv$
Re_{plate}	Reynolds number for flow in the cooling plate
R_{wall}	conduction resistance, $m^2 K/kW$
Sc	Schmidt number, $\mu/\rho D_{aw}$
T	absolute temperature, K
t	thickness of the cooling plate, m
U	overall heat transfer coefficient, $kW/m^2 K$
V	volumetric flow rate, l/min
x	mass fraction of ammonia in the liquid phase
y	mass fraction of ammonia in the vapor phase
$\tilde{x}$	mole fraction of ammonia in the liquid phase
$\tilde{y}$	mole fraction of ammonia in the vapor phase
z	mole fraction of ammonia in the absorbing/desorbing vapor flux

Greek symbols

δ	falling film thickness, m
μ	dynamic viscosity, kg/m s, $N s/m^2$
v	kinematic viscosity, m^2/s
ρ	density, kg/m^3
Γ	mass flow rate of falling film per cooling plate width, kg/m s

Subscripts

C	coolant
film	falling film
film1	falling film
H_2O	water
i	interface
L	liquid phase
NH_3	ammonia
plate	cooling plate
V	vapor phase

Superscript

*	modified

They used a finite volume technique to formulate their model. Kim [13] developed a model based on an integral formulation of momentum, heat and mass transfer equations to compare co-current and counter-current absorbers. Velocity, temperature and concentration profiles were assumed to be parabolic. The flow was assumed to be laminar and fully developed. Further, the coolant wall was assumed to be either adiabatic or isothermal. Perez-Blanco [14], on the other hand, simulated their design model using empirical correlations for the heat and mass transfer coefficients. The model considered was for falling film absorption around coiled tubes. They used a finite difference scheme to solve the model.

In addition, most of these models were developed and analyzed for co-current vapor flow systems [11,12,14]. However, the situation is more complicated for counter-current vapor flow systems. Due to the opposite flow direction of the fluids, inlet conditions need to be defined at opposite ends of the absorber. There are very few models of counter-current absorbers. Kang et al. [9] adapted a model originally developed by Price and Bell [10] for a vertical-fluted tube absorber. They considered a counter-current system under the assumption that weak solution is well mixed, and, consequently, both liquid bulk and liquid–vapor interface are always at thermodynamic equilibrium. Their model neglects the liquid-phase mass transfer resistance. Garimella [8] used similar assumptions in his design model for counter-current vapor flow absorption over very small diameter horizontal tubes. In the literature, models for volatile absorbents which consider the mass transfer resistance in both the liquid and vapor phases are mainly limited to co-current systems. The numerical analysis by Kang et al. [16,17] predicted the required length of the counter-current absorber. Their models considered resistance to mass transfer in both the phases. However, the computational details of the scheme were not provided.

In this paper, a finite difference model is developed for a counter-flow system. The model takes into account the liquid and vapor phase mass transfer resistances, and uses empirical correlations to predict the heat and mass transfer coefficients. Empirical correlations for the heat and mass transfer coefficients are useful for simulating wavy-laminar and turbulent flow conditions, the conditions in which numerically calculated coefficients are less reliable.

2. Mathematical model

A mathematical model for the counter-current falling film absorber was developed. The system considered here consists of an array of cooling plates over which a weak solution is distributed. The weak solution then flows down the cooling surface under the influence of gravity. The absorbate vapor enters from the bottom of the absorber and it flows through the narrow channels formed by an assemblage of cooling plates. The vapor is absorbed by the weak solution flowing counter-current to it. The heat of absorption thus released increases the temperature of the liquid and the vapor streams. The liquid solution is kept under subcooled state by rejecting heat to the coolant fluid, and thereby, the absorption process is sustained. Continuity and energy balance equations are applied at each differential control volume of the absorber, as shown in Fig. 1. The model also accounts for the coupled heat and mass transfer processes accompanying the falling-film absorption.

The following assumptions were made in building the model:

1. The absorption process is assumed to be in steady state.
2. System pressure is constant.
3. Thermodynamic equilibrium exists at the liquid–vapor interface.
4. The heat transfer surface under the conditions is completely wet (i.e. there is no direct heat transfer between the vapor and coolant).
5. Heat losses to the environment are negligible.
6. No flooding occurs between the two adjacent cooling plates.
7. Mass transfer due to thermal and pressure difference is negligible (Mass transfer occurs only due to concentration gradient).
8. Effect of non-absorbable gases is ignored.

The mass transfer between the liquid and vapor phases is due to the combined effect of bulk transport and molecular diffusion of NH_3 and H_2O across the liquid–vapor interface. For steady state, the molar flux of the vapor absorbed by the weak solution is given by [18]

$$\frac{\mathrm{d}m_{\mathrm{NH_3}}}{M_{\mathrm{NH_3}}}+\frac{\mathrm{d}m_{\mathrm{H_2O}}}{M_{\mathrm{H_2O}}}=\mathrm{d}A_{\mathrm{i}}K_{\mathrm{V}}\ln\left(\frac{z-\tilde{y}_i}{z-\tilde{y}}\right) \tag{1}$$

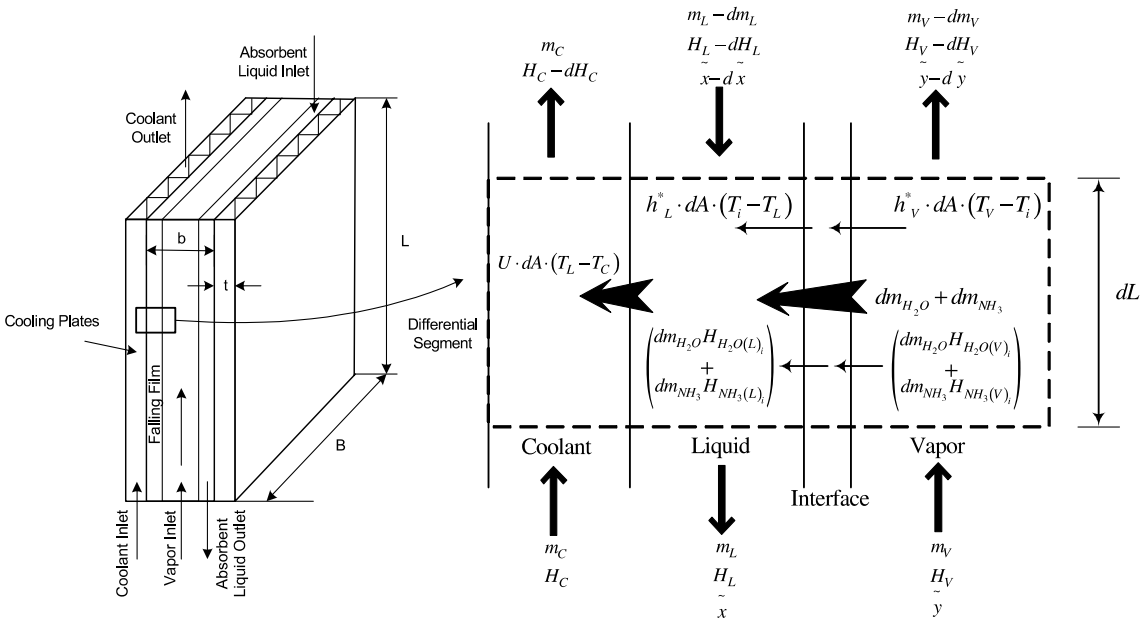

Fig. 1. Schematic of the differential control volume of the absorber.

$$\frac{dm_{NH_3}}{M_{NH_3}} + \frac{dm_{H_2O}}{M_{H_2O}} = dA_i K_L \ln\left(\frac{z-\tilde{x}}{z-\tilde{x}_i}\right) \quad (2)$$

Subscripts L, V, and i denote the liquid, vapor and liquid–vapor interface respectively. The positive value of molar flux, namely dm_{NH_3} and dm_{H_2O} signify the mass transfer from vapor to liquid phase. As both ammonia and water can be absorbed/desorbed, the absorption mass flux consists of both the constituents. The mole fraction of ammonia in the absorbing/desorbing vapor is defined as z and can be expressed by Eq. (3). For ammonia–water pair, the value of z is normally less than the concentration of the vapor stream [6].

$$z = \left(\frac{\frac{dm_{NH_3}}{M_{NH_3}}}{\frac{dm_{H_2O}}{M_{H_2O}} + \frac{dm_{NH_3}}{M_{NH_3}}}\right) \quad (3)$$

Yih and Chen [19] developed the liquid-side mass transfer correlations for laminar, wavy and turbulent falling films. Their model was based on the motion of eddies near the liquid–vapor interface, and the values of constants were obtained by fitting their own experimental data and data provided by ten other researchers. Their correlation is applicable to fully developed conditions only. The correlation was established in the range of $49 < Re_{film1} < 300$, and can be expressed as

$$K_L = (0.01099 Re_{film1}^{0.3955} Sc_L^{0.5}) \left[\frac{D_{aw(L)} M_L}{\rho_L}\left(\frac{g}{\nu_L^2}\right)^{1/3}\right] \quad (4)$$

The convective heat transfer coefficient between the vapor and the interface, h_V is based on the laminar flow conditions inside a parallel plate channel. The correlation assumes uniform surface temperature, and neglects the edge effect due to the finite width of parallel plate channels. Though the correlation is not exactly applicable to finite rectangular ducts, it can be considered a reasonable approximation for large aspect ratio. The relation is also restricted to fully developed profiles of velocity and temperature, and is given by [20]

$$h_V = 7.541\left(\frac{k_V}{D_h}\right) \quad (5)$$

where the hydraulic diameter D_h is defined as

$$D_h = \frac{4(\text{Cross sectional area of the duct})}{(\text{Wetted perimeter})} \quad (6)$$

The similarity between heat and mass transfer processes can be utilized to deduce the analogous heat and mass transfer coefficients [21]. The heat and mass transfer analogy is particularly useful when either one of the heat and mass transfer coefficients is difficult to obtain, and is given by

$$\frac{h}{M} = C_p K \left(\frac{Sc}{Pr}\right)^{2/3} \quad (7)$$

Heat and mass transfer analogy is applied on Yih and Chen's correlation [19] to estimate the convective heat transfer coefficient between the solution and the interface, h_L. Similarly, the vapor-side mass transfer coefficient, K_V is obtained by the application of heat and mass transfer analogy on Eq. (5).

The heat transfer between the liquid and vapor phases occurs due to the combined contribution of convective heat transfer and sensible heat load of the mass transferred across the interface. The ordinary convective heat transfer is due to the temperature gradient between the fluid in motion and the bounding surface. If the convective heat transfer is also accompanied by mass transfer across the bounding surface, an extra amount of heat will transfer due to the heat capacity of the mass being transferred. This sensible heat transfer is primarily due to the temperature gradient between the liquid and vapor phases, and consequently between the liquid, liquid–vapor interface and vapor regimes. The convective heat transfer coefficient can be modified to account for the effect of mass transfer. The modified heat transfer coefficient, h^* for simultaneous heat and mass transfer is given by [18]

$$h^* = h\frac{c}{1-e^{-c}} \quad (8)$$

$$\text{where } c \text{ is, } c = \frac{\frac{dm_{NH_3}}{M_{NH_3}} C_{pNH_3} + \frac{dm_{H_2O}}{M_{H_2O}} C_{pH_2O}}{h} \quad (9)$$

The energy balance equations for the control volumes of liquid and vapor phases are given by

$$m_L H_L + dQ_C = (m_L - dm_L)(H_L - dH_L) + h_L^* \cdot dA(T_i - T_L) + dm_{H_2O} H_{H_2O(L)_i} + dm_{NH_3} H_{NH_3(L)_i} \quad (10)$$

$$m_V H_V = (m_V - dm_V)(H_V - dH_V) + h_V^* \cdot dA(T_V - T_i) + dm_{H_2O} H_{H_2O(V)_i} + dm_{NH_3} H_{NH_3(V)_i} \quad (11)$$

The liquid–vapor interface is assumed to be at thermodynamic equilibrium. Concentration of ammonia in the vapor and liquid at the interface can then be expressed as

$$\tilde{y}_i = f(T_i, P) \quad (12)$$

$$\tilde{x}_i = f(T_i, P) \quad (13)$$

Energy balance at the liquid–vapor interface gives

$$h_L^* \cdot dA(T_i - T_L) + dm_{H_2O} H_{H_2O(L)_i} + dm_{NH_3} H_{NH_3(L)_i} = h_V^* \cdot dA(T_V - T_i) + dm_{H_2O} H_{H_2O(V)_i} + dm_{NH_3} H_{NH_3(V)_i} \quad (14)$$

The heat absorbed by the coolant can be found by an energy balance over the coolant, coolant–liquid interface and global control volumes:

$$dQ_C = U \cdot dA(T_L - T_C) \tag{15}$$

$$dQ_C = m_C dH_C \tag{16}$$

$$dQ_C = (m_L - dm_L)(H_L - dH_L) + m_V H_V - m_L H_L - (m_V - dm_V)(H_V - dH_V) \tag{17}$$

where overall heat transfer coefficient, U combines the various thermal resistances in the path of heat flow between the weak solution and coolant, and can be expressed as

$$\frac{1}{U} = \frac{1}{h_C} + R_{wall} + \frac{1}{h_{film}} \tag{18}$$

In the present model, lamella-type plates are chosen as the cooling plates. These plates have good heat transfer characteristics and are commonly used in falling film chillers. The following correlation was used to compute the coolant-side heat transfer coefficient, h_C [22].

$$h_C = 0.026\left(\frac{k_C}{t}\right) Re_{plate}^{0.82} Pr_C^{0.32} \tag{19}$$

The correlation developed by Wilke [23] is used to calculate the convective heat transfer coefficient between the falling film and the cooling plates. The Wilke correlation is based on experiments for a wide range of Prandtl and Reynold numbers in fully developed regions. It was established for $Re_{film} < 2460 Pr^{-0.646}$, and is given by

$$h_{film} = 1.88\left(\frac{k_L}{\delta}\right) \tag{20}$$

where the average film thickness, δ for the laminar flow is given by [24]

$$\delta = 0.91 Re_{film}^{1/3}\left(\frac{v_L^2}{g}\right)^{1/3} \tag{21}$$

3. Numerical technique

Finite difference method is used to solve the system of nonlinear ordinary differential equations. The model is subjected to the inlet conditions of liquid, vapor and coolant flow regimes. The absorber was divided into differential segments of an incremental length, dL. The system considered here has already been explained in detail. In brief, coolant and vapor are introduced at the bottom and flow upward while the liquid flows down from the top, and hence, the inlet liquid and vapor conditions are known at opposite ends. One way to simulate such finite difference model is to first guess either vapor and coolant conditions at the top section or liquid conditions at the bottom section of the absorber. Then iteratively perform the simulation from the location of assumption to the other end until known inlet conditions are achieved. However, there are three unknowns for each vapor/liquid conditions: temperature, mass flow rate and concentration, and, thus, the iteration has to be done by assuming at least three unknowns.

A simpler way is to calculate the coolant, liquid and vapor conditions for successive states in their respective flow directions. Fig. 2 gives a general idea of the numerical technique. Each incremental segment was further divided into liquid, vapor and coolant differential segments. The model is primarily based on two routines. Routine 1 solves the liquid differential segments by marching in the downward direction, whereas Routine 2 marches upward to solve the vapor and coolant differential segments. Due to the interlinking of the liquid, vapor and coolant control volumes, the vapor and coolant conditions are initially required to solve the liquid region. An initial guess for the conditions of all the vapor and coolant differential segments is taken to be equal to the inlet vapor and coolant conditions. The model loops over these two routines iteratively to achieve better approximations of an unknown solution. This is repeated until all unknown variables converge to stable values. The solution method can be summarized as follows:

1. Assume a length of the absorber and divide the absorber into differential segments of incremental length, dL.
2. Equate the vapor and coolant conditions of all incremental steps to the inlet vapor and coolant conditions.
3. Solve the liquid control volume for each segment by marching downwards. The values of vapor and coolant conditions at each node are obtained by step (2) in case of first iteration or by Routine 2 in case of subsequent iterations. The following steps describe Routine 1:

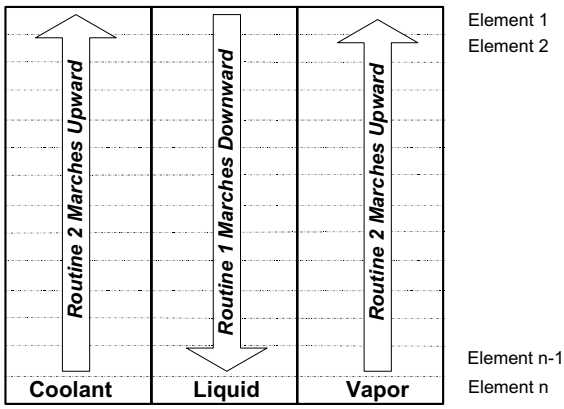

Fig. 2. Schematic of the numerical technique.

i. Guess the liquid–vapor interface temperature, T_i.
ii. Calculate the liquid and vapor side mass fraction of ammonia, x_i and y_i at the interface with Eqs. (12) and (13).
iii. Guess z.
iv. Calculate a new value of z by using Eqs. (1) and (2).
v. If the difference between the old and new values of z is less than the assumed convergence criterion, go to step (vi), otherwise go to step (iii).
vi. Calculate the mass flux of ammonia and water, dm_{NH_3} and dm_{H_2O} using Eqs. (1)–(3).
vii. Calculate a new value of T_i from an energy balance of interface control volume by using Eq. (14).
viii. If the difference between the old and new values of T_i is less than the assumed convergence criterion, go to step (ix), otherwise go to step (i).
ix. Calculate the mass flow rate and concentration of the liquid phase for the next segment.
x. Calculate the enthalpy of liquid phase for the next segment of the incremental steps from an energy balance of liquid control volume with Eq. (10).

4. Solve the vapor and coolant differential segments by marching upward. The values of liquid conditions at each node are obtained by Routine 1. The following steps describe Routine 2:
i. Guess the liquid–vapor interface temperature, T_i.
ii. Calculate the liquid and vapor side mass fraction of ammonia, x_i and y_i at the interface with Eqs. (12) and (13).
iii. Guess z.
iv. Calculate a new value of z by using Eqs. (1) and (2).
v. If the difference between the old and new values of z is less than the assumed convergence criterion, go to step (vi), otherwise go to step (iii).
vi. Calculate the mass flux of ammonia and water, dm_{NH_3} and dm_{H_2O} with Eqs. (1)–(3).
vii. Calculate a new value of T_i from an energy balance of interface control volume by using Eq. (14).
viii. If the difference between the old and new values of T_i is less than the assumed convergence criterion, go to step (ix), otherwise go to step (i).
ix. Calculate the mass flow rate and concentration of the vapor phase for the next segment.
x. Calculate the enthalpy of vapor phase and coolant for the next segment of the incremental steps from an energy balance of the vapor and coolant control volumes with Eqs. (11) and (15).

5. Repeat steps (3) and (4) until rate of change of any variable between two successive iterations is less than 10^{-10}.
6. Check the mass flow rate of vapor at the outlet of absorber. If it is a negative value, decrease the length of the absorber and go to step (2); if it is a positive value and is greater than 0.1% of the inlet vapor flow, increase the length of the absorber and go to step (2); if the value lies between zero and 0.1% of the inlet vapor flow, print the results. This criterion insures that 99.9% of inlet vapor is absorbed in the absorbent liquid.

4. Results and discussion

A computer code was developed which yields the mass flow rate, temperature, and concentration distribution for liquid and vapor phases along the absorber length. In addition, temperature and concentration conditions at the liquid–vapor interface, and heat and mass fluxes across the interface are also obtained. The code also incorporates a check on the occurrence of flooding between the adjacent cooling plates. The flooding criterion used for this purpose is based on the Wallis equation [25]. Overall mass and energy balance were done for each design condition, and accuracies better than 99.995% and 99.7%, respectively were achieved. The model was then used to analyze a lamella plate based absorber with falling film absorption. Fig. 1 shows a schematic diagram of the absorber. The geometric dimensions and operating conditions used in the current analysis are listed in Tables 1 and 2. The operating conditions considered here are the typical conditions encountered in the absorption based combined power/cooling thermodynamic cycle [26].

The results obtained by the computation are summarized in Table 3. The temperature and concentration profiles for the different fluid regions are plotted as a function of axial distance from the top of the absorber. Fig. 3 shows the variation in bulk mean temperature of the coolant, solution and vapor along the absorber length. The solution temperature decreases gradually as the solution flows down in the absorber. Due to the rejection of heat to the coolant, the coolant temperature increases as it flows through the cooling plates. Also note that the interfacial temperature is always greater than the solution temperature. This is due to the gener-

Table 1
Operating conditions of the counter-current absorber

System pressure, bar	2
Coolant medium	Water
Inlet conditions	
Coolant mass flow rate, kg/s	0.504
Coolant bulk temperature, K	302.6
Solution mass flow rate, kg/s	0.02
Solution bulk temperature, K	323
Solution mass fraction	0.25
Vapor mass flow rate, kg/s	0.004
Vapor bulk temperature, K	300
Vapor mass fraction	0.997

Table 2
Geometric dimensions of the counter-current absorber

Cooling plate type	Lamella plates
Cooling plate material	SS 316
Cooling plate width (B), cm	15
Number of cooling plates in a row	4
Spacing between adjacent cooling plates (b), cm	1
Thickness of the cooling plates (t), mm	1.3

Table 3
Design results of the counter-current absorber

Required length of the cooling plates (L), m	1.125
Absorber heat duty, kW	8.34
Outlet conditions	
Coolant bulk temperature, K	306.6
Solution mass flow rate, kg/s	0.024
Solution bulk temperature, K	304.1
Solution mass fraction	0.375
Vapor mass flow rate, kg/s	1.6×10^{-6}
Vapor bulk temperature, K	324.2

ation of absorption heat at the liquid–vapor interface. The difference between the vapor, liquid, liquid–vapor interface and coolant temperatures can lead to the conclusion that the liquid-side heat transfer resistance is negligible in comparison to the other constituents of heat transfer resistance. The coolant-side heat transfer resistance dominates the overall heat transfer resistance at the absorber's upper section. On the vapor side, the vapor temperature increases as it flow in the upward direction and it approaches the interface temperature. Fig. 4 illustrates the mass flow rate of the liquid and vapor phases at various axial positions of the absorber. The flow rate of the vapor decreases as it flows upward in the absorber eventually becoming zero at top of the

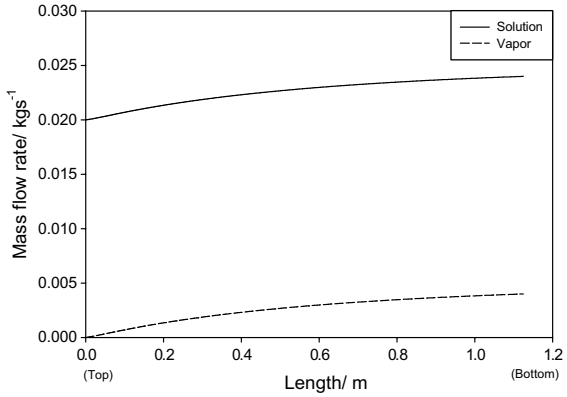

Fig. 4. Variation of mass flow rate along the absorber length.

absorber. This is consistent with the design criterion of complete absorption of the vapor phase. The absorption of vapor results in an increase of the solution flow rate.

The profiles of the concentration of liquid and vapor phases, and the composition of the absorbing flux are shown in Fig. 5. For the design conditions considered, it was found that the molar concentration of ammonia in the absorbing mass flux, z is more than 1 near the inlet vapor region, and thereafter, its value decreases to less than 1. It implies that a small amount of water vapor is being evaporated in the bottom section of the absorbers. Very low concentration of water in the inlet vapor leads to the transfer of water from liquid to vapor phase by diffusion mechanism. The results by Kang et al. [17] and Herbine and Perez-Blanco [27] also confirm that desorption of water can occur near the entrance location of the vapor phase. However, in their case they considered the absorption process in a co-current ammonia–water bubble absorber. The value of z also remains higher than the vapor concentration. The higher concentration of ammonia in the absorbing flux as compared to

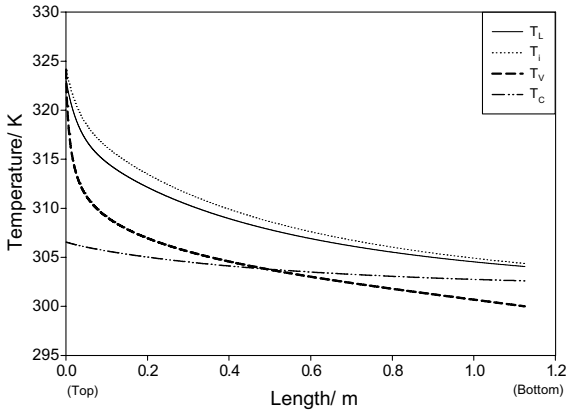

Fig. 3. Variation of temperature along the absorber length.

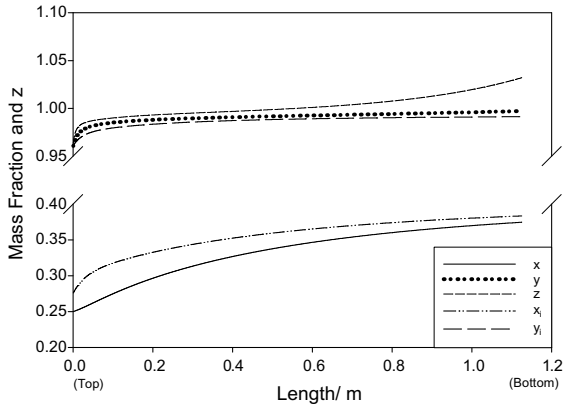

Fig. 5. Variation of concentration along the absorber length.

that in the vapor phase leads to the decrease in vapor mass fraction from the bottom to the top of the absorbers. Similar reasoning stands behind the increase in liquid concentration as it flows in downward direction.

It was also found that the concentration gradient between the vapor and liquid–vapor interface is lower than the gradient between the liquid and liquid–vapor interface. It is evident from the concentration plots as shown in Fig. 5. It implies that for the operating conditions considered, a major fraction of the overall mass transfer resistance lies in the falling film. Kim [13] and Perez-Blanco [14] also considered both the liquid and vapor-side mass transfer resistances in their numerical model, and found liquid-side mass transfer resistance to be dominant.

A parametric analysis was performed to gauge the influence of various parameters on the absorption rate. The baseline design conditions are listed in Table 1. For the existing baseline conditions, the parameters considered are the coolant mass flow rate, coolant inlet temperature and weak solution inlet temperature. The above parameters can be changed by the use of an auxiliary heat exchanger, a coolant pump or a different cooling source.

Many investigators have recommended the use of auxiliary heat exchanger to subcool the weak solution before it enters the absorber. The heat exchanger not only transfers some heat from the weak solution to strong solution but also increases the driving potential to absorb the ammonia. As shown in Figs. 6 and 7, the length required for the complete vapor absorption decreases as the weak solution is subcooled. However, the effect is not too significant. For highly subcooled liquid, the solution temperature increases for a while as the liquid flows down the cooling surface. This is due to the fact that subcooling has a combined contribution on decreasing the heat transfer from liquid to coolant region and increasing the mass transfer from vapor to liquid region. And at the top section of the absorber, heat transfer from liquid to coolant region is less than the heat transferred to liquid phase by heat of absorption.

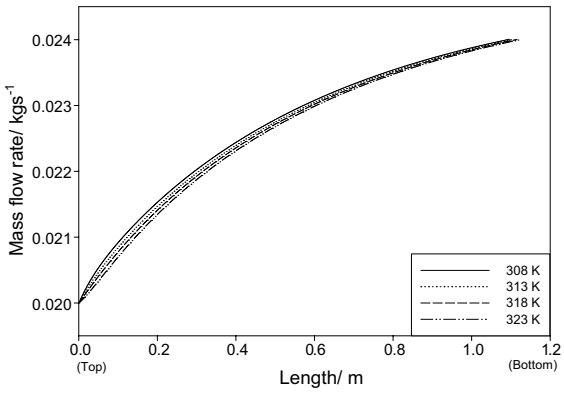

Fig. 7. Variation of solution mass flow rate along the absorber length at various inlet solution temperatures.

The influence of coolant inlet temperature on the size of absorber is illustrated in Figs. 8 and 9. The cooling water inlet temperature range was selected as 297–305.4 °C (75–90 °F), which covers typical thermal conditions of the cooling towers. As expected, decreasing the inlet coolant temperature results in an increase in absorption rate and consequently, decreases the minimum absorber length required for a given mass absorption. The effect is very prominent and can be utilized in places where the option of lower inlet coolant temperature is viable.

Figs. 10 and 11 show the effect of the coolant flow rate on the absorber size. As evident from the plots, the required length decreases as the mass flow rate

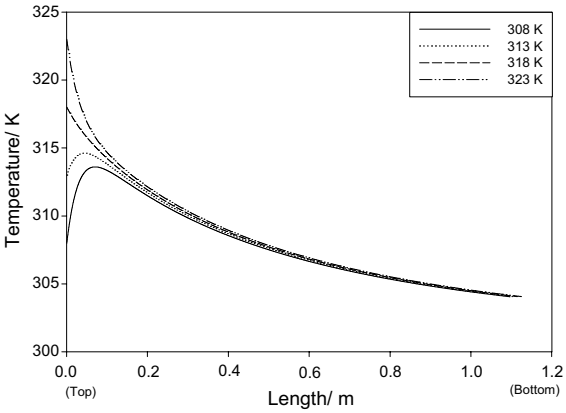

Fig. 6. Variation of solution temperature along the absorber length at various inlet solution temperatures.

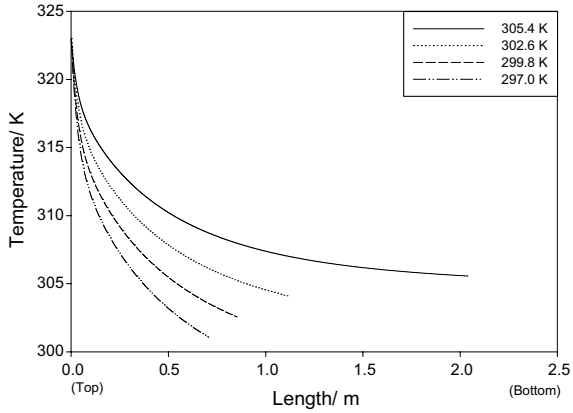

Fig. 8. Variation of solution temperature along the absorber length at various coolant inlet temperatures.

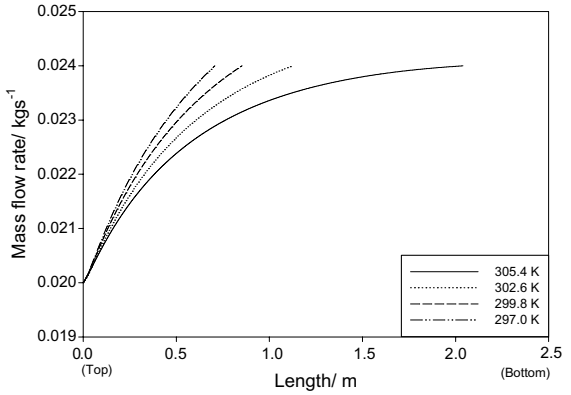

Fig. 9. Variation of solution mass flow rate along the absorber length at various coolant inlet temperatures.

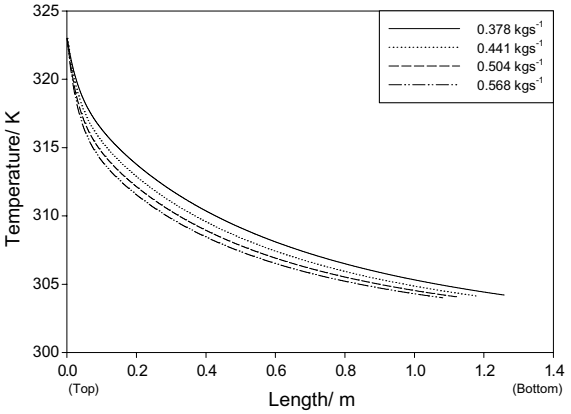

Fig. 10. Variation of solution temperature along the absorber length at various coolant flow rates.

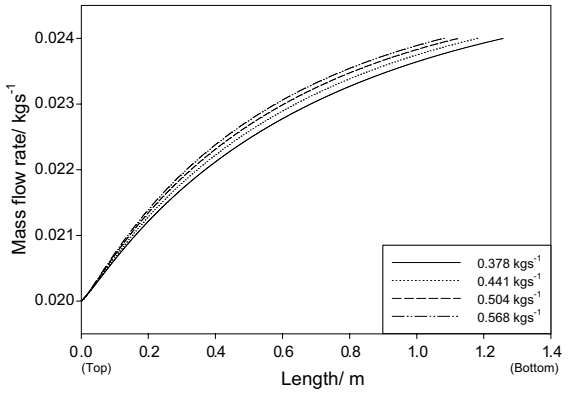

Fig. 11. Variation of solution mass flow rate along the absorber length at various coolant flow rates.

increases. The reason for the decrease in size is the combined contribution of the increase in coolant-side heat transfer coefficient and the decrease in average coolant temperature. The average coolant temperature is decreased because the increase in coolant flow rate will increase the heat capacity of the coolant stream.

5. Conclusion

A numerical technique is presented to model the counter-current flow absorbers while accounting for the liquid and vapor phase mass transfer resistances in the falling film absorption. It also considers the coupled nature of heat and mass transfer processes. For the operating conditions considered, the liquid mass transfer resistance was found to control the overall absorption process. The analysis showed that interface temperature is always greater than the bulk liquid temperature. In addition, the liquid-side heat transfer resistance is negligible in comparison to the other constituents of heat transfer resistance. A parametric analysis was conducted to assess the effect of various parameters on the performance of the absorber. As expected, the absorption rate increases as the coolant inlet and solution inlet temperatures decrease, and as the coolant flow rate increases. However, the effect of coolant flow rate and coolant inlet temperature on the reduction of the absorber's size is found to be more significant than the effect of solution inlet temperature.

References

[1] J.D. Killion, S. Garimella, A critical review of models of coupled heat and mass transfer in falling-film absorption, Int. J. Refrig. 24 (2001) 755–797.
[2] M. Ruheman, The transfer of heat and matter in an ammonia absorber, Trans. Inst. Chem. Eng. (1947) 17–20.
[3] S.W. Briggs, Concurrent, crosscurrent, and countercurrent absorption in ammonia–water absorption refrigeration, ASHRAE Trans. 77 (1) (1971) 171–175.
[4] Y.T. Kang, W. Chen, R.N. Christensen, Design of ammonia–water condenser with a fluted tube, ASHRAE Trans. 102 (2) (1996) 587–595.
[5] Y.T. Kang, W. Chen, R.N. Christensen, Development of design model for a rectifier in GAX absorption heat pump systems, ASHRAE Trans. 102 (1) (1996) 963–972.
[6] Y.T. Kang, W. Chen, R.N. Christensen, A generalized component design model by combined heat and mass transfer analysis in NH_3–H_2O absorption heat pump systems, ASHRAE Trans. 103 (1) (1997) 444–453.
[7] A.P. Colburn, T.B. Drew, The condensation of mixed vapours, AIChE Trans. 33 (1937) 197–212.
[8] S. Garimella, Microchannel components for absorption space-conditioning systems, ASHRAE Trans. 106 (2000) 453–462.

[9] Y.T. Kang, R.N. Christensen, Development of a counter-current model for a vertical fluted tube GAX absorber, in: Proceedings of the ASME International Absorption Heat Pump Conference, 1994, pp. 7–16.
[10] B.C. Price, K.J. Bell, Design of binary vapor condensers using the colburn-drew equations, AIChE Symposium Series-Heat Transfer-Research and Design vol. 70 (138) 1974, pp. 163–171.
[11] K. Gommed, G. Grossman, M.S. Keonig, Numerical model of ammonia–water absorption inside a vertical tube, in: Proceedings of the International Sorption Heat Pump Conference, 1999, pp. 275–281.
[12] K. Gommed, G. Grossman, M.S. Keonig, Numerical study of absorption in a laminar falling film of ammonia–water, ASHRAE Trans. 107 (2001) 453–462.
[13] B. Kim, Heat and mass transfer in a falling film absorber of ammonia–water absorption systems, Heat Transfer Eng. 19 (3) (1998) 53–63.
[14] H.A. Perez-Blanco, A model of an ammonia–water falling film absorber, ASHRAE Trans. 94 (1) (1988) 467–483.
[15] S.V. Potnis, A. Gomezplata, R.A. Papar, G. Anand, D.C. Erickson, GAX component simulation and validation, ASHRAE Trans. 103 (1) (1997) 454–459.
[16] Y.T. Kang, R.N. Christensen, T. Kashiwagi, Ammonia–water bubble absorber with a plate heat exchanger, ASHRAE Trans. 104 (1998) 1565–1575.
[17] Y.T. Kang, A. Akisawa, T. Kashiwagi, Analytical investigation of two different absorption modes: falling film and bubble types, Int. J. Refrig. 22 (2000) 640–649.
[18] R.E. Treybal, Mass Transfer Operations, McGraw-Hill, New York, 1980.
[19] S.M. Yih, K.Y. Chen, Gas absorption into wavy and turbulent falling liquid films in a wetted-wall column, Chem. Eng. Commun. 17 (1982) 123–136.
[20] S. Kakaç, R.C. Shah, W. Aung, Handbook of Single-Phase Convective Heat Transfer, John Wiley & Sons Inc., 1987.
[21] T.H. Chilton, A.P. Colburn, Mass transfer (absorption) coefficients, Ind. Eng. Chem. 26 (1934) 1183–1187.
[22] D. Azbel, Fundamentals of Heat Transfer for Process Engineering, Noyes Publications, Park Ridge, NJ, 1984, p. 382.
[23] W. Wilke, Wärmeübergang an Rieselfilme, VDI-Forschungsheft 490 (1962) B28.
[24] W. Nusselt, VDI-Zeitschrift 54 (1910) 1154.
[25] G.B. Wallis, One-Dimensional Two-Phase Flow, McGraw-Hill, New York, 1969.
[26] G. Tamm, D.Y. Goswami, Novel combined power and cooling thermodynamic cycle for low temperature heat sources, Part II: Experimental investigation, J. Solar Eng. 125 (2003) 223–229.
[27] G.S. Herbine, H. Perez-Blanco, Model of an ammonia–water bubble absorber, ASHRAE Trans. 101 (1995) 1324–1332.